WARSAW UNIVERSITY OF TECHNOLOGY Index 351733
FACULTY OF CIVIL ENGINEERING
COMMITTEE FOR CIVIL AND WATER ENGINEERING
POLISH ACADEMY OF SCIENCES ISSN 1230-2945

DOI: 10.24425/ace.2023.145282

ARCHIVES OF CIVIL ENGINEERING

Vol. LXIX ISSUE 2 2023

pp. 517 –534

Research paper

Experimental study on SHPB cyclic impact of rubber-cement composite with different confine modes

Rongzhou Yang[1], Ying Xu[2], Peiyuan Chen[3], Lin Cheng[4], Jinfu Ding[5], Hongxin Fu[6]

Abstract: To promote the application of rubber-cement composites as the main bearing structure and key components in practical engineering under frequent dynamic disturbances, in this work, the split Hopkinson pressure bar (SHPB) cyclic impact tests of rubber-cement composite specimens with four different confine modes were carried out in which the impact load increased sequentially. The relationship between average strain rate, ultimate strain and impact times and the relationship between peak stress, damage energy, ultimate strain and incident energy were analyzed. The results showed that the appropriate confine reinforcement treatment can make rubber-cement composite give full play to its deformation ability when it was completely damaged. Carbon fiber-reinforced polymer (CFRP) sheet and steel cylinder can work together with the rubber-cement composite matrix to resist impact load, which effectively improves the structural strength, damage fracture energy, and cyclic impact resistance of the rubber-cement composite. Finally, based on the effect difference of confine modes, the simplified plane force models of rubber-cement composite specimens with four different confine modes were established, which clearly revealed the completely different impact resistance mechanism of the rubber-cement composites with different constraints under cyclic impact loading.

Keywords: split Hopkinson pressure bar (SHPB), carbon fiber-reinforced polymer (CFRP), rubber-cement composite, cyclic impact, damage fracture energy, impact resistance

[1]PhD., Eng., State Key Laboratory of Mining Response and Disaster Prevention and Control in Deep Coal Mines, School of Civil Engineering and Architecture, Anhui University of Science and Technology, Huainan 232001, China, e-mail: rongzhouy@outlook.com, ORCID: 0000-0002-0126-2446

[2]PhD., Eng., State Key Laboratory of Mining Response and Disaster Prevention and Control in Deep Coal Mines, School of Civil Engineering and Architecture, Anhui University of Science and Technology, Huainan 232001, China, e-mail: yxu@aust.edu.cn, ORCID: 0000-0001-8438-3130

[3]Assoc. Prof., PhD., School of Civil Engineering and Architecture, Anhui University of Science and Technology, Huainan 232001, China, e-mail: peiyuan29@126.com, ORCID: 0000-0002-5538-617X

[4]Master's degree, School of Civil Engineering and Architecture, Anhui University of Science and Technology, Huainan 232001, China, e-mail: 13695542763@163.com, ORCID: 0000-0001-5007-8381

[5]Bachelor's degree, School of Civil Engineering and Architecture, Anhui University of Science and Technology, Huainan 232001, China, e-mail: 172094202@qq.com, ORCID: 0000-0003-4246-1617

[6]Bachelor's degree, School of Civil Engineering and Architecture, Anhui University of Science and Technology, Huainan 232001, China, e-mail: hxfuah@foxmail.com, ORCID: 0000-0003-3302-3455

1. Introduction

With the rapid development of the automobile industry, hundreds of millions of waste tires have been produced all over the world, which makes the resource utilization of waste tires become an issue of common concern all over the world [1]. At present, due to the unreasonable disposal of a large number of waste tires, "black pollution", waste of resources, and safety problems are becoming more and more serious [2]. Fortunately, mixing waste tire rubber particles into normal cement-based materials to prepare rubber cement composites/rubber cement-based materials can become a feasible method for recycling waste tire rubber and protecting the environment [3]. Some previous studies have shown that rubber-cement composites are green and sustainable impact-resistant cement-based materials, which have a broad application prospect in earthquake resistance [4], bridge piers [5], and roads [6] because of their outstanding cushioning energy dissipation and anti-fatigue properties.

To better apply rubber-cement composites to practical projects disturbed by frequent shocks, researchers have done a lot of research work on the dynamic mechanical properties and dynamic response characteristics of rubber-cement composites. Pan et al. [7] through the split Hopkinson pressure bar (SHPB) impact simulation test, the dynamic characteristics of rubber concrete under different strain rates were studied, and a mesoscopic model which can accurately predict the static and dynamic characteristics of rubber concrete was established. Lai et al. [8] used the SHPB test system to carry out the high strain rate impact compression test of fiber-reinforced rubberized concrete, and the research showed that it is a promising material for structural resistance to impact and explosive loading. Subashree and Thenmozhi [9] used the drop weight test system to study the impact resistance and energy absorption performance of rubber concrete slabs. Liu et al. [10] used the SHPB test system to study the dynamic compression performance of rubber-modified self-compacting concrete with waste tires under multiple impact loads. The study showed that the addition of rubber aggregate improves the material's resistance to multiple impact loads, deformation resistance, and energy absorption capacity.

However, rubber concrete still has a long way to go in practical application because the low strength and fatigue damage accumulation of rubber-cement composites under cyclic impact can not be used as the main bearing structure and key components under frequent dynamic disturbance. Due to the superior mechanical properties of fiber-reinforced polymer (FRP) and steel cylinder/steel tube materials, FRP and steel cylinder/steel tube are widely used as reinforcement materials in civil engineering [11, 12]. Researchers have also done a lot of research work on the dynamic mechanical properties and dynamic response characteristics of carbon fiber-reinforced polymer (CFRP) and steel cylinder/steel tube reinforced concrete materials. Maazoun et al. [11] studied the bond interaction mechanism between CFRP and concrete under explosive loading and determined the parameters that affect the bond strength between CFRP and concrete under explosive loading. Xiong et al. [13] used the SHPB test system to study the high strain rate compression behav-

ior of CFRP-confined concrete. Xiao et al. [14] used the SHPB test system to study the mechanical behavior of concrete-filled steel tubes under high strain rate compression and discusses the confinement stress and the confinement coefficient under high strain rate loading. Mastor et al. [15] carried out an experimental study on the performance of rubberized pozzolanic concrete-filled hollow steel columns under monotonous and cyclic lateral loads. The results show that when the axial load is 20%, the energy dissipation capacity of rubberized pozzolanic concrete-filled hollow steel column increases the most.

Many studies have shown that [16–19] for rock and concrete materials, the SHPB is a widely used, reliable and safe scientific test system to study the dynamic mechanics and damage characteristics of materials under high strain rate. Based on the above research, in this work, combined with the previous research work [20], the rubber-cement composite was strengthened by combining the superior mechanical properties of CFRP and steel cylinder. The SHPB cyclic impact tests of rubber-cement composite specimens with four different confine modes were carried out in which the impact load increased sequentially. The relationship between average strain rate, ultimate strain and impact times and the relationship between peak stress, damage energy, ultimate strain and incident energy were analyzed. Finally, based on the effect difference of confine modes, the simplified plane force models of rubber-cement composite specimens with four different confine modes were established. The purpose of this paper is to promote the application of rubber-cement composites as the main bearing structure and key components in practical engineering under frequent dynamic disturbances.

2. General situation of test and analysis of calculation principle

2.1. SHPB test system

The schematic diagram of the SHPB test system used in the test is shown in Fig. 1. The physical and technical parameters of the bars and gauges in SHPB are listed in Table 1.

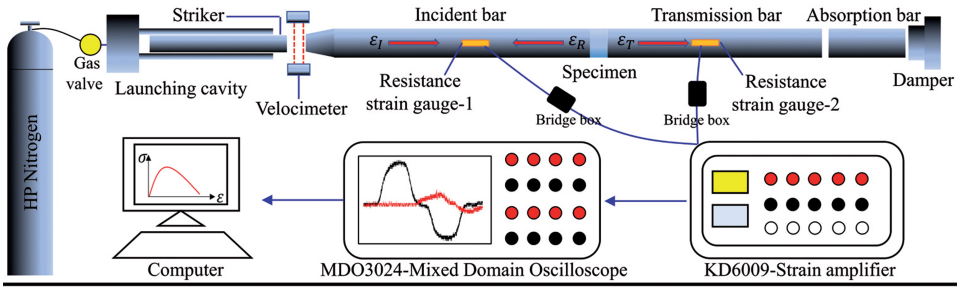

Fig. 1. SHPB test system

Table 1. Physical and technical parameters of the bars and gauges in SHPB [21]

Parameter	Incident & transmission bars	Parameter	Resistance strain gauge
Diameter (mm)	50	Resistance value (Ω)	120 ± 1
Wave velocity (m/s)	5190		
Young's modulus (GPa)	210	Sensitivity coefficient	2 ± 0.01
Density (g/cm^3)	7.8		

2.2. Stress balance analysis and processing method

Stress balance error analysis can effectively reflect the stability and reliability of data in the process of SHPB testing [22,23]. For this reason, the dynamic wave balance analysis of the SHPB system in the empty bar (No specimen) state was carried out, as shown in Fig. 2. According to the observation for Fig. 2, it was known that the stress waves basically reached the stress balance during the SHPB test, and it was proved that the results of this study are reliable. What needs further consideration is that Fig. 2b showed that there was a small fluctuation error in the reflected wave curve. To avoid this error, the calculation formulas of strain rate, strain, and stress under the two-wave method composed of the incident wave and transmitted wave were used in the experimental data processing. The equation of the two-wave method under cyclic impact compression is as follows [24]:

$$\begin{cases} \varepsilon_{i+1} = \dfrac{2C\displaystyle\int_0^t \left(\varepsilon_{I(i+1)} - \varepsilon_{T(i+1)}\right) \mathrm{d}t}{L_{S(i-1)} - \varepsilon_i L_{S(i-1)}} \\ \dot{\varepsilon}_{i+1} = \dfrac{2C\left(\varepsilon_{I(i+1)} - \varepsilon_{T(i+1)}\right)}{L_{S(i-1)} - \varepsilon_i L_{S(i-1)}} \\ \sigma_{i+1} = \dfrac{4AE}{\pi D_{Si}^2}\varepsilon_{T(i+1)} \end{cases} \tag{2.1}$$

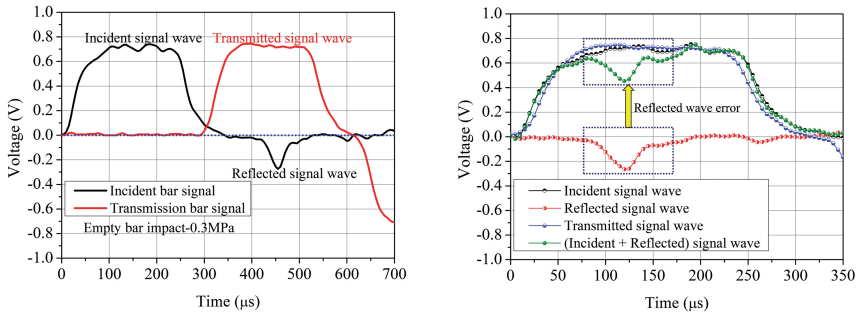

(a) (b)

Fig. 2. Stress balance analysis in SHPB test: (a) typical three-wave graphs; and (b) stress uniformity verification

where: E – elastic modulus of compression bar, A – cross-sectional area of compression bar, C – wave velocity of compression bar, ε_{i+1} – compressive strain of the specimen under the $(i+1)$-th cycle impact, $\dot{\varepsilon}_{i+1}$ – compressive strain rate of the specimen under the $(i+1)$-th cycle impact, σ_{i+1} – compressive stress of the specimen under the $(i+1)$-th cycle impact, $\varepsilon_{I\,(i+1)}$ – incident strain of the incident bar under the $(i+1)$-th cycle impact, $\varepsilon_{T\,(i+1)}$ – the transmission strain of the transmission bar under the $(i+1)$-th cycle impact, D_{Si} – diameter of specimen under the i-th cycle impact, $L_{S(i-1)}$ – length of the specimen under the $(i-1)$-th cycle impact (When $i = 0$, then $L_{S(-1)} = L_{S0}$, L_{S0} is the initial diameter of the specimen).

2.3. Energy calculation principle

During the SHPB test, the process of energy propagation and energy conversion is as follows (Fig. 3): (1) The incident wave σ_I carries the incident energy W_I to the contact surface $X1$ and generates the reflected wave σ_R and transmitted wave σ_{T1} at the contact surface $X1$. The reflected wave σ_R carries the reflected energy W_R and propagates in the opposite direction. (2) The transmitted wave σ_{T1} carries the remaining energy and propagates along the positive direction and penetrates the specimen to the contact interface $X2$. Similarly, the transmitted wave σ_{T1} produces a transmitted wave σ_{T2} at the contact interface $X2$. (3) The transmitted wave σ_{T2} carries the transmitted energy W_T and continues to propagate in the positive direction to the absorption bar and the damper. Therefore, in the process of SHPB one-dimensional stress wave propagation, it is mainly accompanied by incident energy W_I, reflected energy W_R, transmitted energy W_T, and damage energy W_D, including ejection kinetic energy W_K, sound energy $W_{\text{Sound energy}}$, thermal energy $W_{\text{Thermal energy}}$, and radiant energy $W_{\text{Radiant energy}}$ [25].

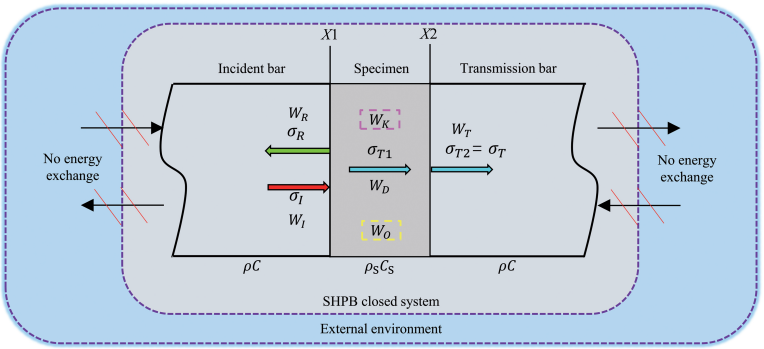

Fig. 3. Principle schematic diagram of stress wave propagation and energy dissipation in SHPB test

The principles of stress wave propagation and energy dissipation in SHPB test are as follows [22]: The wave impedance (ρC) of SHPB is larger than that ($\rho_S C_S$) of the specimen, which results in the mismatch of the wave impedance between the SHPB and the specimen, which leads to the reflection and transmission of stress waves on the contact surfaces $X1$ and $X2$. According to the law of conservation of energy, "the change of the total energy

of a system can only be equal to the amount of energy coming into or out of the system, and the total energy is the sum of the mechanical energy, thermal energy, and any form of internal energy except thermal energy of the system". The whole SHPB test system can be regarded as a closed thermodynamic system (Fig. 3). Then, in the process of SHPB testing, the incident energy must be transformed into other different forms of energy and dissipated with the propagation of stress waves and the motion of the bars.

According to the two-wave method [22], the equations for calculating the incident energy, reflection energy and transmission energy under cyclic impact compression can be further deduced:

$$W_{Ii} = AEC \int_0^t \varepsilon_{Ii}^2 \, \mathrm{d}t \tag{2.2}$$

$$W_{Ri} = AEC \int_0^t \left(\varepsilon_{Ii}^2 + \varepsilon_{Ti}^2 - 2\varepsilon_{Ii}\varepsilon_{Ti} \right) \mathrm{d}t \tag{2.3}$$

$$W_{Ti} = AEC \int_0^t \varepsilon_{Ti}^2 \, \mathrm{d}t \tag{2.4}$$

where: W_{Ii} – incident energy under the i-th cycle impact, W_{Ri} – reflection energy under the i-th cycle impact, W_{Ti} – transmission energy under the i-th cycle impact.

According to the kinetic energy theorem, the equation for calculating the ejection kinetic energy of fragments in case of failure is [25]:

$$W_{K,\mathrm{Total}} = \sum_i^n W_{Ki} \rightarrow W_{Ki} = \sum_j^x W_{Ki,j} = \frac{1}{2} \sum_j^x m_{ij} v_{ij}^2 \tag{2.5}$$

where: $W_{K,\mathrm{Total}}$ – total fragment ejection kinetic energy of the specimen during the whole SHPB cycle impact tests, W_{Ki} – fragment ejection kinetic energy of the specimen under the i-th cycle impact, m_{ij} – mass of the j-th fragment under the i-th cyclic impact, v_{ij} – ejection velocity of the j-th fragment under the i-th cyclic impact.

The thermal energy, sound energy, and radiant energy in the SHPB test process are called other energy, so the calculation method of other energy is [25]:

$$W_{O,\mathrm{Total}} = \sum_i^n W_{Oi} \rightarrow W_{Oi} = W_{\mathrm{Thermal\ energy},i} + W_{\mathrm{Sound\ energy},i} + W_{\mathrm{Radiant\ energy},i} + \ldots \tag{2.6}$$

where: $W_{O,\mathrm{Total}}$ – other energy during the whole SHPB cycle impact tests, W_{Oi} – other energy under the i-th cycle impact, $W_{\mathrm{Thermal\ energy},i}$ – thermal energy under the i-th cycle impact, $W_{\mathrm{Sound\ energy},i}$ – sound energy under the i-th cycle impact, $W_{\mathrm{Radiant\ energy},i}$ – radiant energy under the i-th cycle impact.

According to the law of conservation of energy, the equation for calculating the damage energy of specimens under cyclic impact load is [25]:

$$W_{D,\text{Total}} = \sum_{i}^{n} W_{Di} \rightarrow W_{Di} = W_{Ii} - W_{Ri} - W_{Ti} - W_{Ki} - W_{Oi} \tag{2.7}$$

where: $W_{D,\text{Total}}$ – total damage energy of the specimen during the whole SHPB cycle impact tests, W_{Di} – damage energy of the specimen under the i-th cycle impact.

In the process of energy calculation, it is worth further exploring that the presence or absence of specimens has a completely different influence on the stress wave propagation and energy conversion in SHPB (Fig. 4). The state of stress wave propagation and energy conversion in SHPB without specimen is shown in Fig. 4a. In the case of no specimen placed in the SHPB, the materials of the incident bar and the transmission bar are the same, which makes the wave impedance of the incident bar and the transmission bar match completely, thus causing the incident wave to be almost completely converted into the transmitted wave [22]. However, it is still possible that the end faces of the incident bar and the transmission bar are not in full contact, resulting in a slightly reflected wave due to the inclusion of air medium between the ends of the two bars, which is equivalent to changing the cross-sectional area ratio between the incident bar and the transmission bar. The state of stress wave propagation and energy conversion in SHPB with specimens is shown in Fig. 4b. When the specimen is placed between the incident bar and the transmission bar, the wave impedances of both the incident bar and the transmission bar can not match the wave impedances of the specimen, which causes the incident wave to be mainly converted into reflected wave and transmitted wave [22,24]. It should be noted that no matter whether

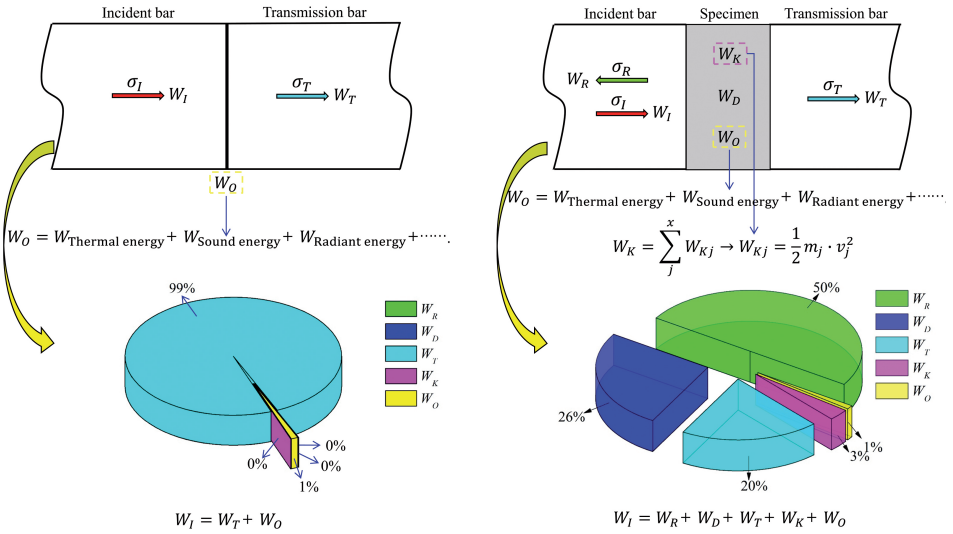

Fig. 4. The mechanism of energy dissipation and the distribution of different energies in SHPB test: (a) empty bar test; and (b) specimen test [22,25]

there are specimens in SHPB or not, there will be dissipation of other energy in the impact process, and the default in the discussion is that the dissipation values of other energy with and without specimens are equal.

From the relevant literature [25, 26], it can be seen that in the process of SHPB and explosion impact, the kinetic energy of the specimen fragments is very small, accounting for no more than 5% of the input energy. At the same time, other energy is even less than the kinetic energy of the fragments. To calculate the damage energy of the specimen under cyclic impact load, the ejection kinetic energy and other energy which account for a very small proportion can be ignored. It is also known that the integral area of the stress-strain curve is the damage energy per unit volume of the specimen, so the damage energy of the specimen under cyclic impact load is [27]:

$$W_{Di} = V_{S0} \int_0^{\varepsilon} \sigma_i \, \mathrm{d}\varepsilon_i = W_{Ii} - W_{Ri} - W_{Ti} \tag{2.8}$$

where: V_{S0} – initial volume of the specimen. In the process of calculating the damage energy, to facilitate the calculation, it can be assumed that the volume of the specimen remains unchanged during the whole cyclic impact process.

2.4. Test materials and specimen preparation

The raw materials used in the test were mainly mix proportion materials and confine materials, as shown in Table 2 and 3. The grain size distribution curves of the river sand and rubber particles for the test and the mass mix proportion design of rubber-cement composite are shown in the Fig. 5. Mass mix proportion: water (1) cement (2): rubber particles (0.52): river sand (2.8) [28]. The preparation process of specimens was mainly divided into two stages: (1) the preparation of rubber-cement composite specimens (Fig. 6) and (2) the confines of rubber-cement composite specimens (Fig. 7).

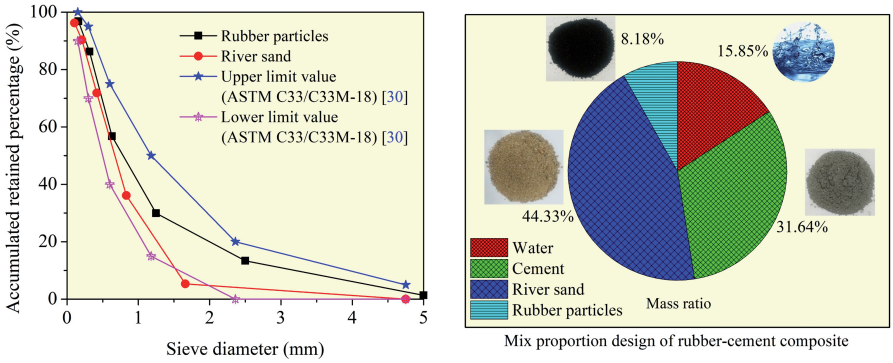

(a) (b)

Fig. 5. (a) The grain size distribution curves of the river sand and rubber particles for the test and (b) the mix proportion design of rubber-cement composite

Table 2. Physical parameters of mix proportion raw materials [29]

Parameter	Cement	Parameter	River sand	Parameter	Waste tire rubber particles
Type specification	P·O 42.5	Density (kg/m^3)	2600	Surface geometry	Irregular polyhedron
Compressive strength (MPa) – 28 days	> 42.5	Fineness modulus	2.60	Density (kg/m^3)	1120

Table 3. Physical parameters of confine materials and CFRP sheet impregnated adhesive

Parameter [29]	CFRP sheet	Parameter	CFRP sheet impregnated adhesive	Parameter	Steel cylinder
Theoretical thickness (mm)	0.111	Composition	(1) Epoxy resin, (2) Curing agent	Height (mm)	100.50
Tensile strength (MPa)	3325	Mixed proportion	2(1):1(2)	Thickness (mm)	1.96
Elastic modulus (MPa)	$2.40 \cdot 10^5$	Design value of shear strength (MPa)	18	Inner diameter (mm)	51.67
Elongation (%)	1.74	Solid content (%)	99.6	Density (g/cm^3)	7.85

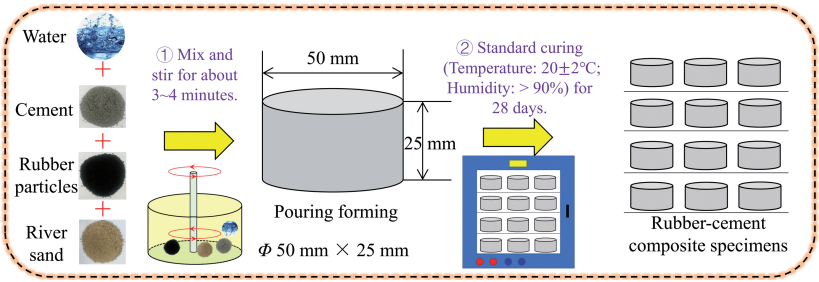

Fig. 6. Preparation of rubber-cement composite specimens

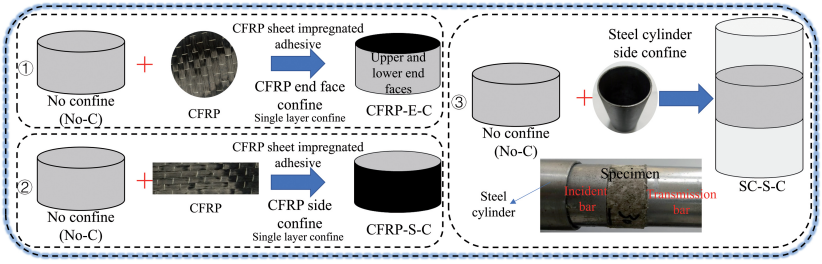

Fig. 7. Confines of rubber-cement composite specimens

2.5. Test methods and results

In this work, the cyclic impact tests of the specimens (No-C, CFRP-E-C, CFRP-S-C, and SC-S-C) were carried out in which the impact load increased sequentially. Specifically, the impact pressure of the first impact compression was 0.2 MPa, the impact pressure of the second impact compression was 0.3 MPa, and the impact pressure of the third impact compression was 0.4 MPa, and so on, until the specimen was completely damaged. The test results show that (Fig. 8), the cyclic impact times of No-C, CFRP-E-C, CFRP-S-C, and SC-S-C were 3, 4, 4, and 7, respectively.

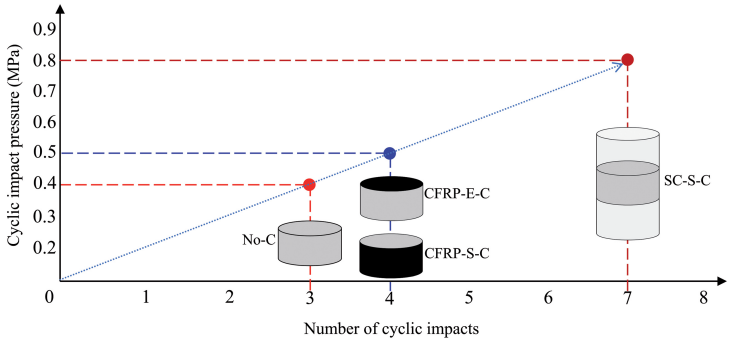

Fig. 8. Cyclic impact results of specimens with four different confine modes

3. Analysis of SHPB test results

3.1. Energy validity verification

To ensure the validity of the test, it is necessary to judge the stability of the incident energy through the relationship between the incident energy and the cycle impact pressure/cycle impact times, and then verify the validity of the incident energy. Fig. 9 shows

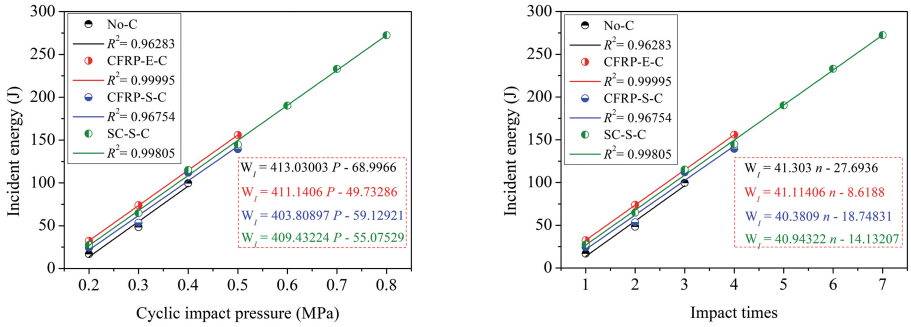

Fig. 9. Energy validity verification: (a) incident energy and cyclic impact pressure; and (b) incident energy and cyclic impact times

that there was an ideal positive proportional relationship between the incident energy and the cycle impact pressure/cycle impact times, and the incident energy fitting curves of specimens No-C, CFRP-E-C, CFRP-S-C, and SC-S-C were almost parallel to each other, which undoubtedly showed the effectiveness of the incident energy. Furthermore, it can effectively analyse the evolution characteristics of various energies of specimens in the process of cyclic impact, which provides a guarantee for effectively exploring the damage evolution of specimens in the process of cyclic impact from the perspective of energy.

3.2. Relationship between average strain rate, ultimate strain and impact times

The relationship between the average strain rate, ultimate strain and impact times of the specimens under four different confine modes during the cyclic impact test is shown in Fig. 10. It can be seen from Fig. 10 that there was an ideal linear relationship between the average strain rate, ultimate strain and impact times, and the correlation coefficient $R^2 > 0.9$. With the synchronous increase of impact times and impact load, the average strain rate and ultimate strain increased synchronously, and the ultimate strain showed

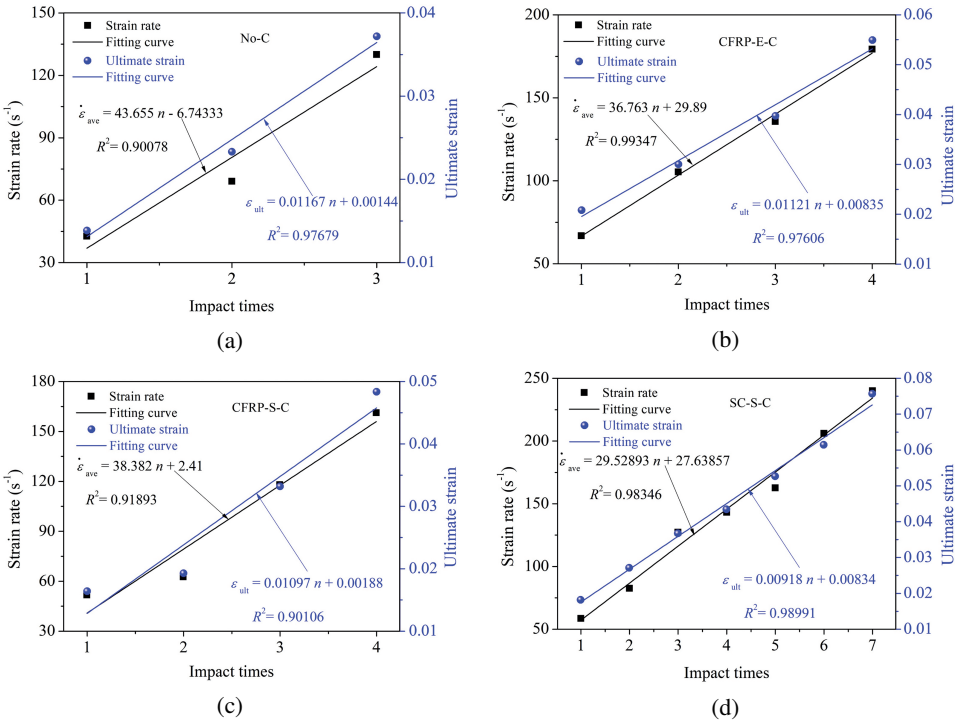

Fig. 10. Relationship between average strain rate, ultimate strain and impact times: (a) No-C; (b) CFRP-E-C; (c) CFRP-S-C; and (d) SC-S-C

an obvious strain rate effect. According to Eqs. (3.1) and (3.2), the cumulative average strain rate and cumulative ultimate strain of the specimen under cyclic impact load can be calculated, as shown in Fig. 11. As can be seen from Fig. 11, the cumulative average strain rate and the cumulative ultimate strain showed a completely consistent change with the change of confining conditions. Compared with specimen No-C, the cumulative ultimate strains of specimens CFRP-E-C, CFRP-S-C, and SC-S-C increased by 95.75%, 57.71%, and 324.20% respectively, which greatly improved the ultimate deformation capacity. It was undeniable that the ultimate deformation of the specimen with the confine of the steel cylinder was much better than that of the CFRP sheet, which showed that the appropriate confine reinforcement treatment can make rubber-cement composite gave full play to its deformation ability when it was completely damaged.

$$\dot{\varepsilon}_{\text{ave, Total}} = \sum_{i}^{n} \dot{\varepsilon}_{\text{ave},i} \tag{3.1}$$

$$\varepsilon_{\text{ult, Total}} = \sum_{i}^{n} \varepsilon_{\text{ult},i} \tag{3.2}$$

where: $\dot{\varepsilon}_{\text{ave, Total}}$ – cumulative average strain rate of the specimen during the whole cyclic impact process, $\varepsilon_{\text{ult, Total}}$ – cumulative ultimate strain of the specimen during the whole cyclic impact process, $\dot{\varepsilon}_{\text{ave},i}$ – average strain rate of the specimen at the i-th cycle impact, $\varepsilon_{\text{ult},i}$ – ultimate strain of the specimen at the i-th cycle impact.

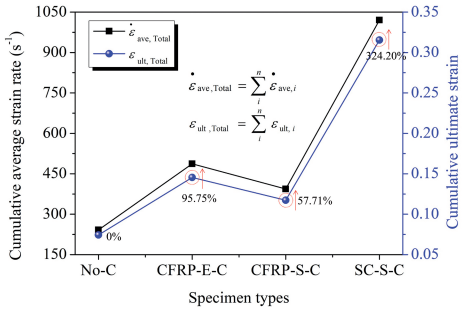

Fig. 11. Cumulative average strain rate and cumulative ultimate strain

3.3. Relationship between peak stress, damage energy, ultimate strain and incident energy

In the process of material deformation caused by an external load, the energy of material failure is input into the material. Therefore, for cement-based materials, the failure of materials is nothing more than that the material exceeds the ultimate stress, ultimate strain, and ultimate damage fracture energy under the action of external load. Then, it is particularly important to explore the relationship between the peak stress, damage energy, ultimate strain and incident energy of the specimen under cyclic impact load. The relationship between peak stress, damage energy, ultimate strain and incident energy is shown in Fig. 12.

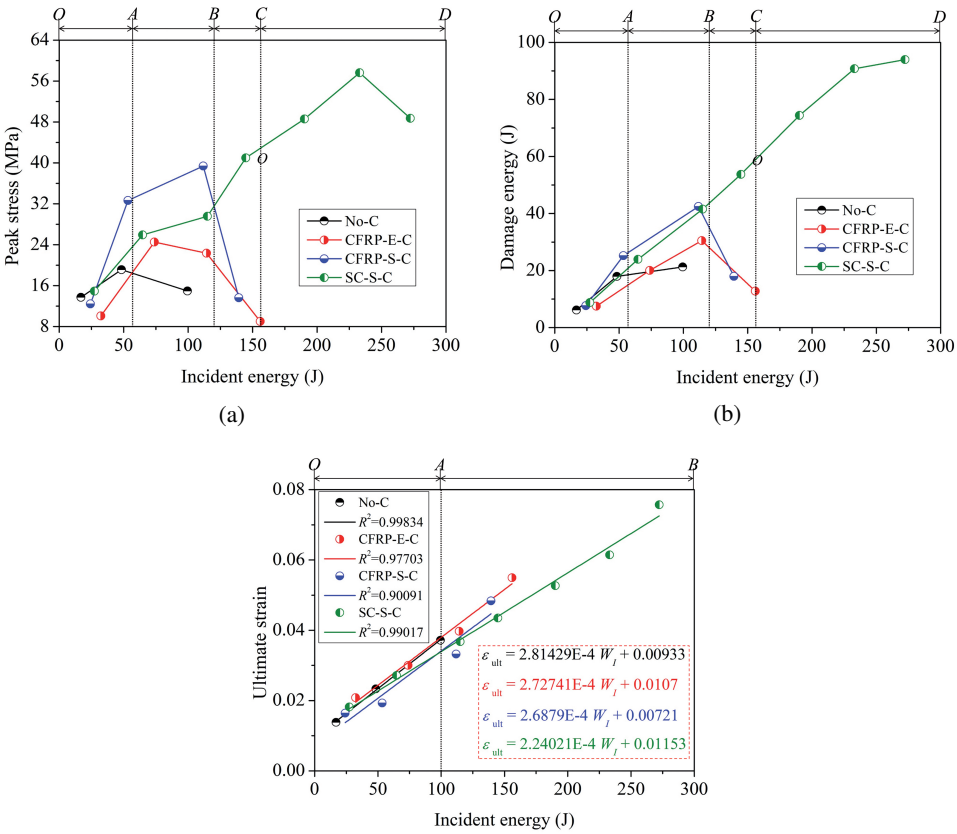

Fig. 12. Relationship between (a) peak stress, (b) damage energy, (c) ultimate strain and incident energy

Fig. 12a and 12b shows that the peak stress and damage energy of the specimens with four different confine modes showed a consistent evolution trend, that was, the peak stress and damage energy of the specimens basically showed a trend of "increase at first and then decrease" with the increase of cyclic incident energy. The variation trends of peak stress and damage energy with incident energy can be divided into four evolution stages: *OA*, *AB*, *BC*, and *CD*.

In the *OA* stage, on the whole, it can be found that the peak stress of the specimen CFRP-E-C was the smallest, the peak stress of the specimen CFRP-S-C was the largest, and the peak stress of the specimens No-C and SC-S-C were in the middle and there was little difference. In the *AB* stage, the growth rate of peak stress decreased, even the peak stress of specimens No-C and CFRP-E-C decreased, and the peak stress of specimen No-C was lower than that of specimen CFRP-E-C. In the *BC* stage, the peak stress of specimen No-C disappeared (complete failure), and the peak stress of specimens CFRP-E-C and

CFRP-S-C decreased rapidly. In the *CD* stage, the peak stress of specimens CFRP-E-C and CFRP-S-C disappeared (complete failure), and the peak stress of specimen SC-S-C increased continuously, but the peak stress of specimen SC-S-C decreased under the seventh impact.

Figure 12c shows that the ultimate strain of the specimens with four different confine modes increased linearly with the increase of cyclic incident energy. The variation trends of ultimate strain with incident energy can be divided into two evolution stages: *OA* and *AB*.

In the *OA* stage, on the whole, the order of the ultimate strain at the same incident energy level was: CFRP-E-C>No-C>SC-S-C>CFRP-S-C. In the *AB* stage, the ultimate strain of specimen No-C disappeared (complete failure), and the ultimate strain of specimens CFRP-E-C, CFRP-S-C, and SC-S-C increased continuously, but the ultimate strain of specimens CFRP-E-C and CFRP-S-C reached the maximum under the fourth impact and then disappeared (complete failure). The difference was that the ultimate strain of the specimen SC-S-C can still continue to increase.

3.4. Analysis and discussion of key issues

According to the analysis results and phenomena in "3.3. Relationship between peak stress, damage energy, ultimate strain and incident energy", the following three key issues were illustrated:

1. In the initial stage, the reason why the peak stress and ultimate strain of specimen CFRP-E-C are the minimum and the maximum respectively is that: The density, modulus, and wave impedance of CFRP sheet and CFRP sheet impregnated adhesive (after curing) are lower than those of rubber-cement composite, which leads to the relatively large compaction effect of CFRP sheet and CFRP sheet impregnated adhesive on the end face of CFRP-E-C in the first impact process, hinders the propagation of stress wave and increases the reflection of the stress wave. In the following stage, the compression effect of specimen CFRP-E-C in the first impact and the restraint crack resistance of CFRP sheet on the end face of rubber-cement composite ensure the propagation of stress wave under the second and third impacts, so that the peak stress of CFRP-E-C is greater than that of specimen No-C.
2. In the process of the first three impact energy inputs, the reasons why the peak stress and ultimate strain of the specimen SC-S-C are less than and larger than the specimen CFRP-S-C respectively are as follows: (1) For the specimen SC-S-C, there is a very small gap between the rubber-cement composite and the steel cylinder at the beginning, resulting in the steel cylinder can not well restrain the transverse expansion deformation of the rubber-cement composite during the first two impacts. It was not until the third impact that the rubber-cement composite had a better extrusion effect with the steel cylinder due to sufficient transverse expansion deformation, thus giving full play to the restraint effect of the steel cylinder. However, this process also caused serious damage to the rubber-cement composite. (2) The difference is that for specimen CFRP-S-C, the CFRP sheet is in close contact with the side of the rubber-cement composite at the beginning. When the axial load is applied, the CFRP sheet and the side of the specimen

will produce extrusion immediately, which effectively prevents the lateral expansion deformation of the rubber-cement composite and reduces the damage degree.

3. In the whole process of impact energy inputs, the reasons why the peak stress and ultimate strain of specimen CFRP-E-C are always less than and larger than specimens CFRP-S-C and SC-S-C, respectively, are as follows: (1) The damage of rubber-cement composite under impact compression load often occurs on the side first because of transverse expansion deformation. Compared with specimen CFRP-E-C, for the specimens CFRP-S-C and SC-S-C, CFRP and steel cylinder directly restrain the side of rubber-cement composite, which restrains the occurrence and development of the damage to a great extent. (2) Although the CFRP sheet and CFRP sheet impregnated adhesive of the end face of the specimen CFRP-E-C had a relatively large compaction effect in the first impact process, the CFRP sheet and CFRP sheet impregnated adhesive of the end face always existed, so the wave impedance mismatch issue between the CFRP sheet and CFRP sheet impregnated adhesive and rubber-cement composite always existed.

3.5. Simplified plane force models

To analyze the force characteristics of different confined rubber-cement composite under cyclic impact load, the three-dimensional specimen was simplified to the two-dimensional plane specimen, and the plane force analysis was carried out, which more clearly highlighted the completely different impact resistance mechanism of different confined rubber-cement composite under cyclic impact load, as shown in Fig. 13.

1. Under the impact load, specimen No-C mainly uses the axial structural resistance F_A and the radial structural resistance F_L produced by the rubber-cement composite matrix in the Y and X directions to resist the axial impact load F and the radial expansion tension F_E respectively.
2. Under the impact load, in addition to the structural resistance of the rubber-cement composite matrix, specimen CFRP-E-C also mainly uses the radial end friction force F_{C-E} generated by the CFRP sheet in the X direction to resist the radial expansion tension F_E.
3. Under the impact load, in addition to the structural resistance of the rubber-cement composite matrix, specimen CFRP-S-C also mainly uses the radial passive confining pressure F_{C-C} produced by the CFRP sheet in the X direction to resist the radial expansion tension F_E.
4. Under the impact load, in addition to the structural resistance of the rubber-cement composite matrix, specimen SC-S-C also mainly uses the radial passive confining pressure F_{S-C} produced by the CFRP sheet in the X direction to resist the radial expansion tension F_E.

From the above plane force analysis, it can be seen that the CFRP sheet and the steel cylinder can control the radial expansion deformation by providing the rubber-cement composite matrix with end friction and passive confining pressure. CFRP sheet and steel cylinder can work together with the rubber-cement composite matrix to resist impact load, which effectively improves the structural strength, damage energy, and cyclic impact resistance of the rubber-cement composite.

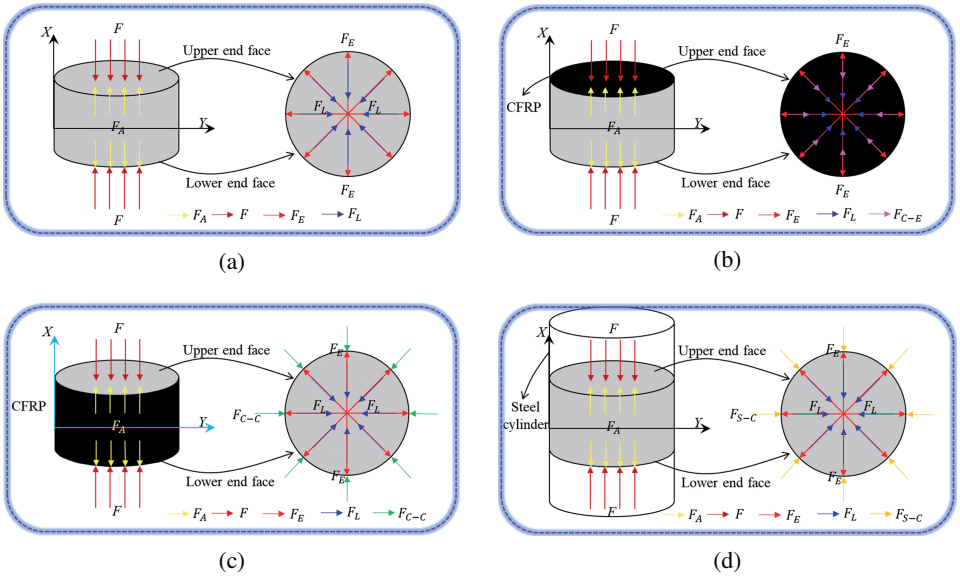

Fig. 13. Simplified plane force states of specimens with four different confine modes: (a) No-C; (b) CFRP-E-C; (c) CFRP-S-C; and (d) SC-S-C

4. Conclusions

In this work, the cyclic impact tests of rubber-cement composite specimens with four different confine modes were carried out in which the impact load increased sequentially. The following conclusions were drawn:

1. With the synchronous increase of impact times and impact load, the average strain rate and ultimate strain increased synchronously, and the ultimate strain showed an obvious strain rate effect. The appropriate confine reinforcement treatment can make rubber-cement composite gave full play to its deformation ability when it was completely damaged.
2. The peak stress and damage energy of the specimens basically showed a trend of "increase at first and then decrease" with the increase of cyclic incident energy. The variation trends of peak stress and damage energy with incident energy can be divided into four evolution stages. The variation trends of ultimate strain with incident energy can be divided into two linear evolution stages.
3. Based on the effect difference of confine modes, the simplified plane force models of rubber-cement composite with different confines under cyclic impact loading were established. From the simplified plane force models, it can be seen that the CFRP sheet and steel cylinder can work together with the rubber-cement composite matrix to resist impact load, which effectively improves the structural strength, damage energy, and cyclic impact resistance of the rubber-cement composite.

Acknowledgements

The authors gratefully acknowledge the financial support from the Scientific Research Foundation for High-level Talents of Anhui University of Science and Technology (2022yjrc84).

References

[1] A. Mohajerani, L. Burnett, J.V. Smith, S. Markovski, G. Rodwell, M.T. Rahman, H. Kurmus, M. Mirzababaei, A. Arulrajah, S. HoWRPibulsuk, and F. Maghool, "Recycling waste rubber tyres in construction materials and associated environmental considerations: A review", *Resources, Conservation and Recycling*, vol. 155, 2020, doi: 10.1016/j.resconrec.2020.104679.

[2] K. Shahzad and Z. Zhao, "Experimental study of NaOH pretreated crumb rubber as substitute of fine aggregate in concrete", *Construction and Building Materials*, vol. 358, 2022, doi: 10.1016/j.conbuildmat.2022.129448.

[3] J. Kang, Y. Liu, J. Yuan, C. Chen, L. Wang, and Z. Yu, "Effectiveness of surface treatment on rubber particles towards compressive strength of rubber concrete: A numerical study on rubber-cement interface", *Construction and Building Materials*, vol. 350, 2022, doi: 10.1016/j.conbuildmat.2022.128820.

[4] I. Khan, K. Shahzada, T. Bibi, A. Ahmed, and H. Ullah, "Seismic performance evaluation of crumb rubber concrete frame structure using shake table test", *Structures*, vol. 30, pp. 41–49, 2021, doi: 10.1016/j.istruc.2021.01.003.

[5] B. Liu, S. Yang, W. Li, and M. Zhang, "Damping dissipation properties of rubberized concrete and its application in anti-collision of bridge piers", *Construction and Building Materials*, vol. 236, 2020, doi: 10.1016/ j.conbuildmat.2019.117286.

[6] R. Pacheco-Torres, E. Cerro-Prada, F. Escolano, and F. Varela, "Fatigue performance of waste rubber concrete for rigid road pavements", *Construction and Building Materials*, vol. 176, pp. 539–548, 2018, doi: 10.1016/j.conbuildmat.2018.05.030.

[7] L. Pan, H. Hao, J. Cui, and T.M. Pham, "Numerical study on dynamic properties of rubberised concrete with different rubber contents", *Defence Technology*, (in press), 2022, doi: 10.1016/j.dt.2022.04.007.

[8] D. Lai, C. Demartino, and Y. Xiao, "High-strain rate compressive behavior of fiber-reinforced rubberized concrete", *Construction and Building Materials*, vol. 319, 2022, doi: 10.1016/j.conbuildmat.2021.125739.

[9] P. Subashree and R. Thenmozhi, "Experimental study of hybrid rubberized composite slabs", *Archives of Civil Engineering*, vol. 64, no. 4, pp. 21–29, 2018, doi: 10.2478/ace-2018-0060.

[10] Z. Liu, X. Chen, X. Wang, and H. Diao, "Investigation on the dynamic compressive behavior of waste tires rubber-modified self-compacting concrete under multiple impacts loading", *Journal of Cleaner Production*, vol. 336, 2022, doi: 10.1016/j.jclepro.2021.130289.

[11] A. Maazoun, S. Matthys, B. Belkassem, O. Atoui, and D. Lecompte, "Experimental study of the bond interaction between CFRP and concrete under blast loading", *Composite Structures*, vol. 277, 2021, doi: 10.1016/j.compstruct.2021.114608.

[12] K.A. Farhan and M.A. Shallal, "Experimental behaviour of concrete-filled steel tube composite beams", *Archives of Civil Engineering*, vol. 66, no. 2, pp. 235–251, 2020, doi: 10.24425/ace.2020.131807.

[13] B. Xiong, C. Demartino, and Y. Xiao, "High-strain rate compressive behavior of CFRP confined concrete: Large diameter SHPB tests", *Construction and Building Materials*, vol. 201, pp. 484–501, 2019, doi: 10.1016/ j.conbuildmat.2018.12.144.

[14] Y. Xiao, J. Shan, Q. Zheng, B. Chen, and Y. Shen, "Experimental studies on concrete filled steel tubes under high strain rate loading", *Journal of Materials in Civil Engineering*, vol. 21, no. 10, pp. 569–577, 2009, doi: 10.1061/(ASCE)0899-1561(2009)21:10(569).

[15] M.N.M.A. Mastor, M.A.A. Kadir, N. Zuhan, K.A. Mujedu, M.Z. Ramli, R.P. Jaya, N.M. Noor, and M.S.A. Shah, "Performance of rubberized concrete-filled hollow steel column under monotonic and cyclic loadings", *Archives of Civil Engineering*, vol. 68, no. 1, pp. 519–538, 2022, doi: 10.24425/ace.2022.140183.

[16] R. Chmielewski, L. Kruszka, R. Rekucki, and K. Sobczyk, "Experimental investigation of dynamic behavior of silty sand", *Archives of Civil Engineering*, vol. 67, no. 1, pp. 481–498, 2021, doi: 10.24425/ace.2021.136484.

[17] L. Liu and H. M. An, "Experimental study of compressive failure of concrete under static and dynamic loads", *Archives of Civil Engineering*, vol. 66, no. 3, pp. 427–441, 2020, doi: 10.24425/ace.2020.134406.

[18] K. Xia and W. Yao, "Dynamic rock tests using split Hopkinson (Kolsky) bar system – A review", *Journal of Rock Mechanics and Geotechnical Engineering*, vol. 7, no. 1, pp. 27–59, 2015, doi: 10.1016/j.jrmge.2014.07.00810.1016/ j.jrmge.2014.07.008.

[19] Y.X. Zhou, K. Xia, X.B. Li, H.B. Li, G.W. Ma, J. Zhao, Z.L. Zhou, and F. Dai, "Suggested methods for determining the dynamic strength parameters and mode-I fracture toughness of rock materials", *International Journal of Rock Mechanics and Mining Sciences*, vol. 49, pp. 105–112, 2012, doi: 10.1016/j.ijrmms.2011.10.004.

[20] R.-Z. Yang, Y. Xu, and P.-Y. Chen. "Dynamic response characteristics of CFRP/steel-cylinder confined rubber cement mortar based on cyclic impact loading", *Magazine of Civil Engineering*, vol. 119, no. 3, 2023.

[21] R. Yang, Y. Xu, and P.Y. Chen, "Experimental study on dynamic stability of rubber-cement composites by SHPB and high-speed slicing", *Archives of Civil Engineering*, vol. 68, no. 1, pp. 319–334, 2022, doi: 10.24425/ ace.2022.140170.

[22] F.Y. Lu, R. Chen, Y.L. Lin, P.D. Zhao, and D. Zhang, *Hopkinson bar techniques*. Beijing: Science Press, 2013.

[23] G. Xue, E. Yilmaz, G. Feng, S. Cao, and L. Sun, "Reinforcement effect of polypropylene fiber on dynamic properties of cemented tailings backfill under SHPB impact loading", *Construction and Building Materials*, vol. 279, 2021, doi: 10.1016/j.conbuildmat.2021.122417.

[24] R. Yang, Y. Xu, P. Chen, and J. Wang, "Experimental study on dynamic mechanics and energy evolution of rubber concrete under cyclic impact loading and dynamic splitting tension", *Construction and Building Materials*, vol. 262, 2020, doi: 10.1016/j.conbuildmat.2020.120071.

[25] R. Shu, T. Yin, X. Li, Z. Yin, and L. Tang, "Effect of thermal treatment on energy dissipation of granite under cyclic impact loading", *Transactions of Nonferrous Metals Society of China*, vol. 29, no. 2, pp. 385–396, 2019, doi: 10.1016/S1003-6326(19)64948-4.

[26] Z.X. Zhang, S.Q. Kou, L.G. Jiang, and P.-A. Lindqvist, "Effects of loading rate on rock fracture: fracture characteristics and energy partitioning", *International Journal of Rock Mechanics and Mining Sciences*, vol. 37, no. 5, pp. 745–762, 2000, doi: 10.1016/S1365-1609(00)00008-3.

[27] Y. Xu and R. Yang, "Dynamic mechanics and damage evolution characteristics of rubber cement mortar under different curing humidity levels", *Journal of Materials in Civil Engineering*, vol. 32, no. 10, 2020, doi: 10.1061/(ASCE)MT.1943-5533.0003351.

[28] R. Yang, Y. Xu, Q. Zheng, P. Chen, and J. Wang, "Fatigue and damage evolution characteristics of rubber cement mortar under graded constant load cyclic compression", *Journal of Building Materials*, vol. 24, no. 5, pp. 961–969, 2021, doi: 10.3969/j.issn.1007-9629.2021.05.009.

[29] R. Yang, P. Chen, J. Ge, Y. Xu, J. Wang, J. Liu, and H. Xie, "Fatigue characteristics of CFRP sheet confined rubber cement mortar under increasing amplitude cyclic load", *Materials Reports*, vol. 36, no. 9, pp. 227–236, 2022, doi: 10.11896/cldb.21040223.

[30] Standards United States, "ASTM C33/C33M-18 Standard specification for concrete aggregate", West Conshohocken, United States, 2018, doi: 10.1520/C0033_C0033M-18.

Received: 2022-11-10, Revised: 2023-03-07